Stellar population of the Rosette Nebula

Kora Muzic

CENTRA - Center for
Astrophysics and Gravitation,
University of Lisbon, Portugal

kmuzic@sim.ul.pt

with V. Almendros Abad, H. Bouy, K. Kubiak, K. Peña Ramírez, A. Krone-Martins, A. Moitinho, & M. Conceição

Motivation

- Most star-forming regions appear to be clumpy, with their populations distributed in several subclusters (e.g. Kuhn et al. 2014, 2021)
- **Monolithic** versus **hierarchical cluster formation**: a tendency towards merging into larger clusters, or dispersal of individual subclusters?
- Studies of the **internal dynamics, mass, and age distribution** of star-forming regions are necessary to shed light on their origins

Credit: Shawn Nielsen

Rosette Nebula

- distance ~1500 pc
- central bubble: NGC 2244 (~2 Myr)
- ongoing star formation associated with the molecular cloud

for the substellar population see poster #144

Membership with Probabilistic Random Forest

Probabilistic Random Forest (PRF; Reis et al. 2019) in short:

- supervised machine learning classifier
- each datapoint represented by a probability density distribution
  - measurement errors taken into account
  - no special treatment necessary for the missing data

Input:
- Multi-band optical/NIR photometry
- Proper motions and parallax (Gaia EDR3)

Training set classes

Members (500 sources):
- X-ray and MIR-excess sources (Bell et al. 2013, Meng et al. 2017)
- known OB stars
- Hα emitters from spectroscopy (Fig 1.) and photometry
- proper motion & parallax consistent with the region, red in various color-magnitude diagrams (CMDs)

Field (~9700 sources)
- inconsistent proper motion
- blue in various CMDs

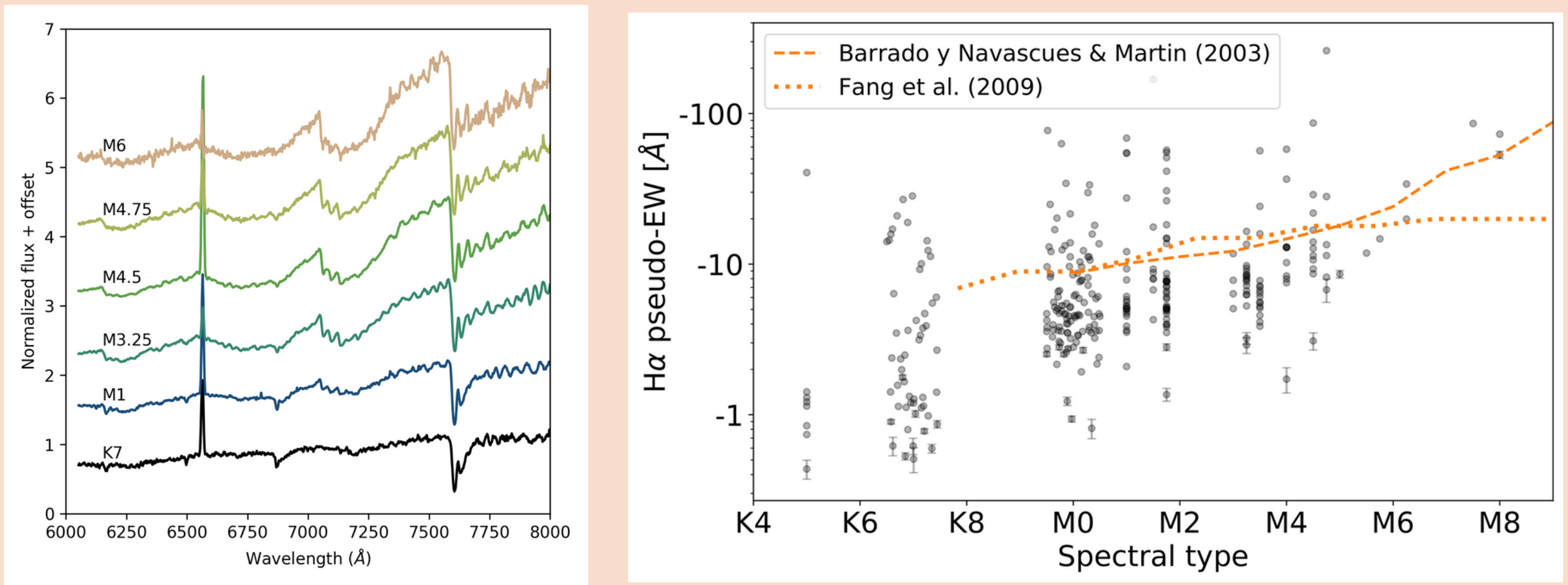

Figure 1. Left: A set of low-mass stellar spectra with strong Hα emission towards the Rosette Nebula, taken with VIMOS/VLT. **Right**: Hα pseudo-EWs as a function of spectral type, obtained from the VIMOS spectra. The sources located above the orange lines have Hα levels consistent with accretion, which is a clear sign of youth.

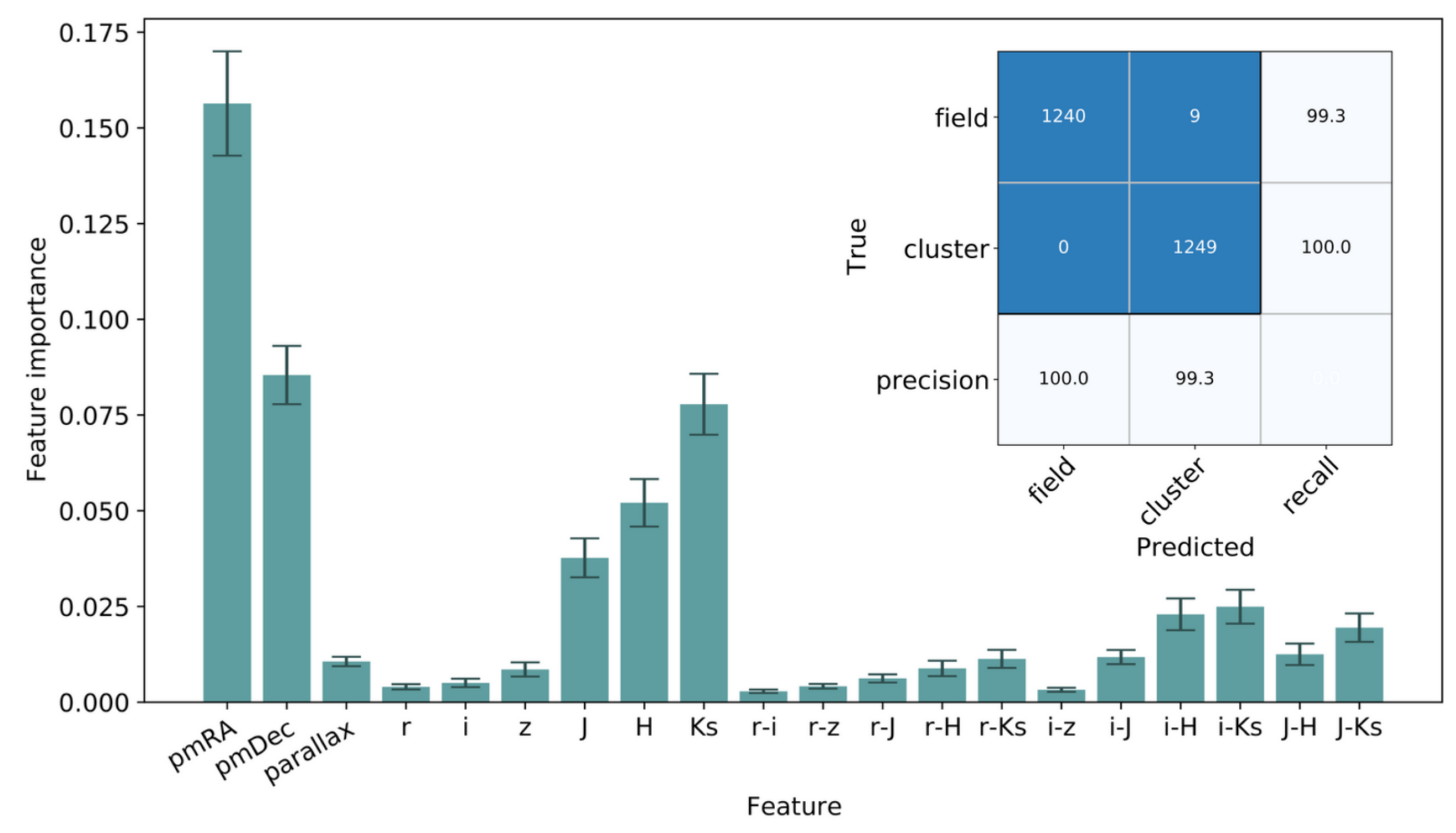

Figure 2. Feature importance, along with the confusion matrix for one of our PRF classifiers. The class imbalance was treated by resampling.

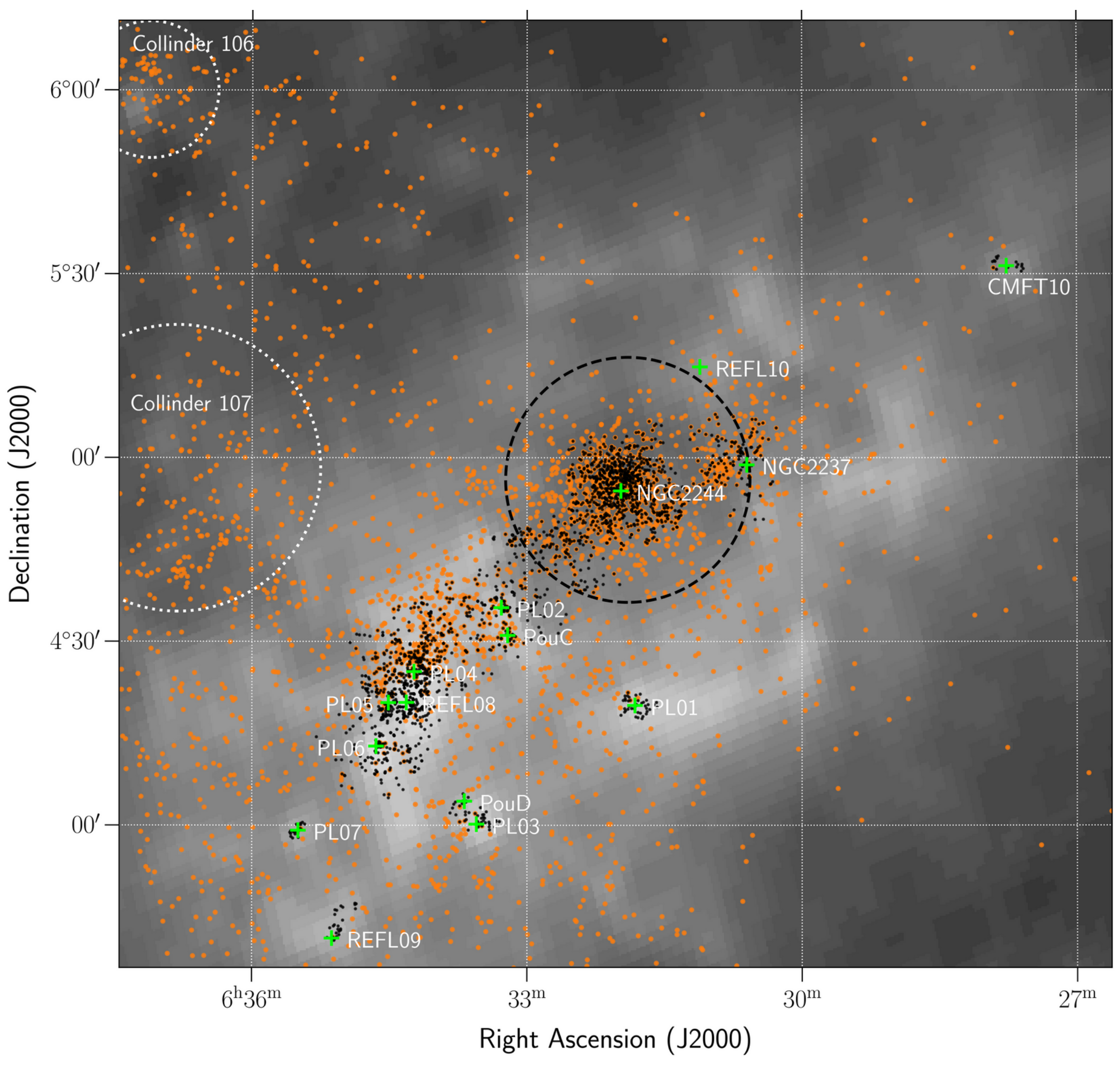

The final list of members

~3000 probable members (PRF probability > 0.8)

Of these, ~1200 are in NGC 2244, with ~55% new

Figure 3. Planck 857 GHz image of the studied region, along with the candidates with membership probability > 0.8 (orange dots), and the mid-infrared and X-ray selected YSOs (black dots).

NGC 2244 relative proper motions

Expansion pattern with the mean radial proper motion component of **1.0 ± 0.1 km/s**

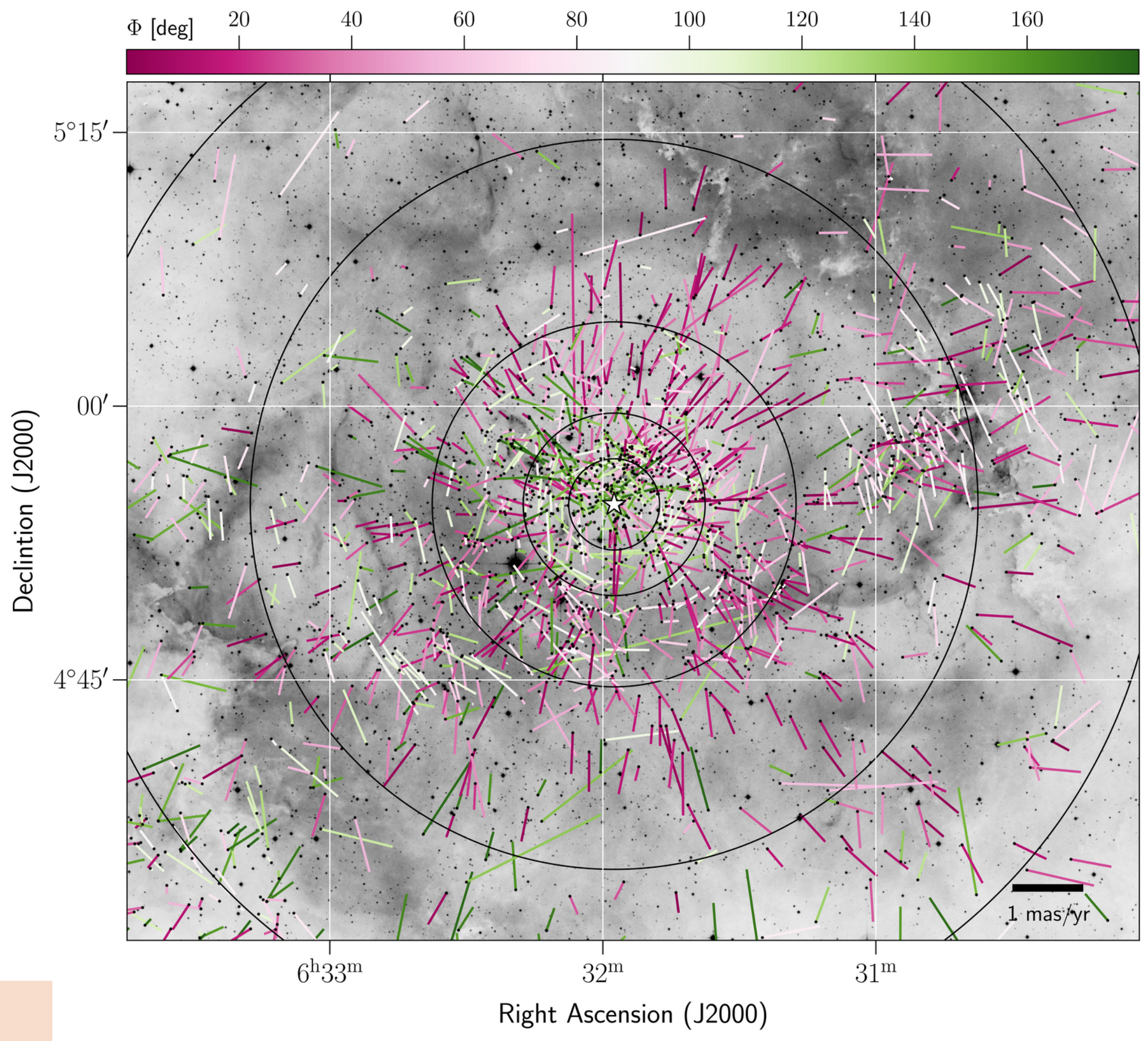

Figure 4. Proper motions relative to the mean motion of the cluster NGC 2244. The origin of each vector is at star's position (black dot) and the color coding is according to the angle between each vector and the line that connects its star with the centre of the cluster. The purple hues highlight the objects with a dominant component pointing radially away from the centre.

Mass and age distributions

- Effective temperature and extinction: SED fitting using VOSA (Bayo et al. 2008)
- Masses and ages: from Hertzprung-Russell (HR) diagram (Fig. 5)

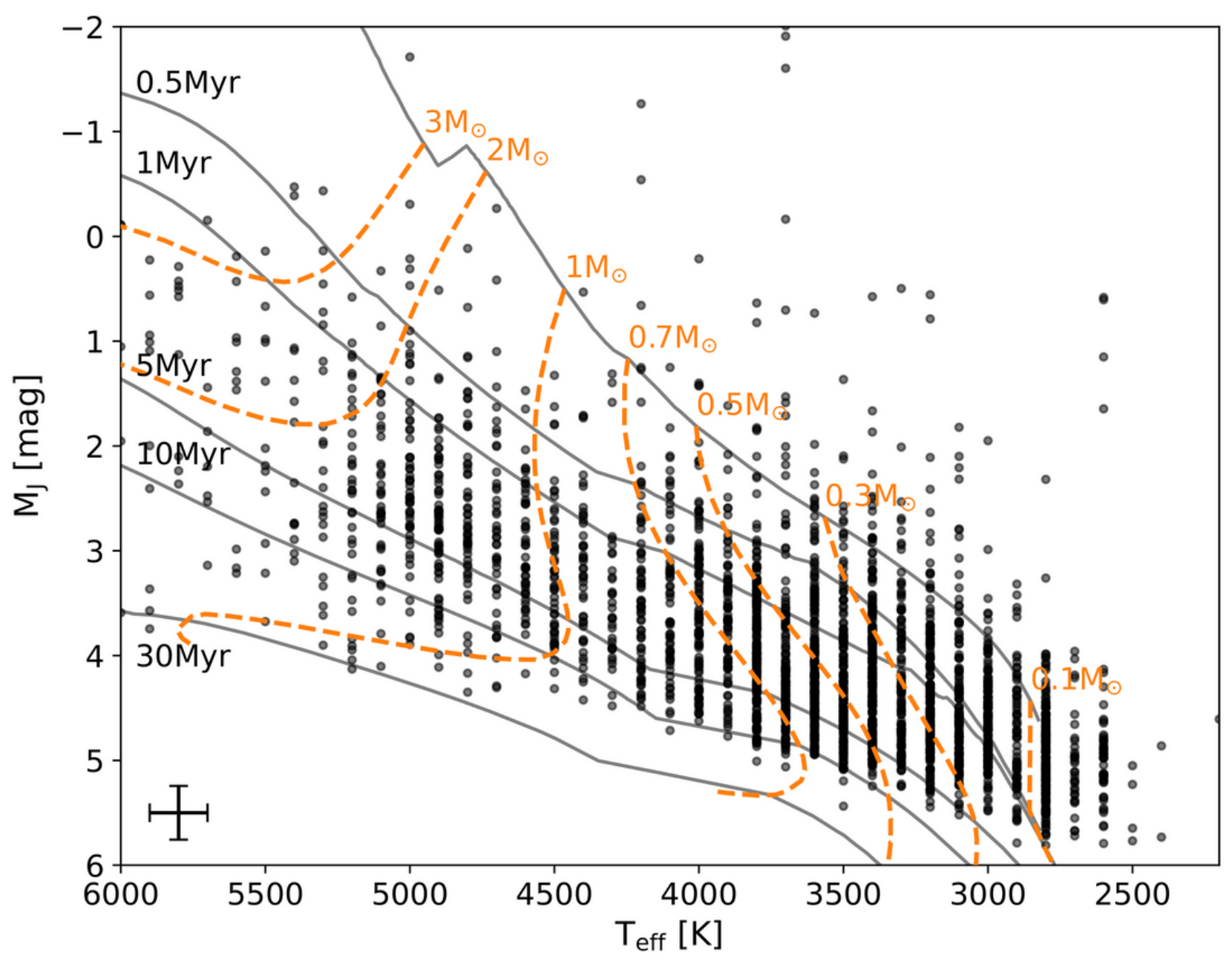

Figure 5. Low-mass part of the HR diagram, showing the high-probability candidate members. The isochrones (grey solid lines) and the lines of constant mass (dashed orange lines) are from the PARSEC series (Bressan et al. 2012).

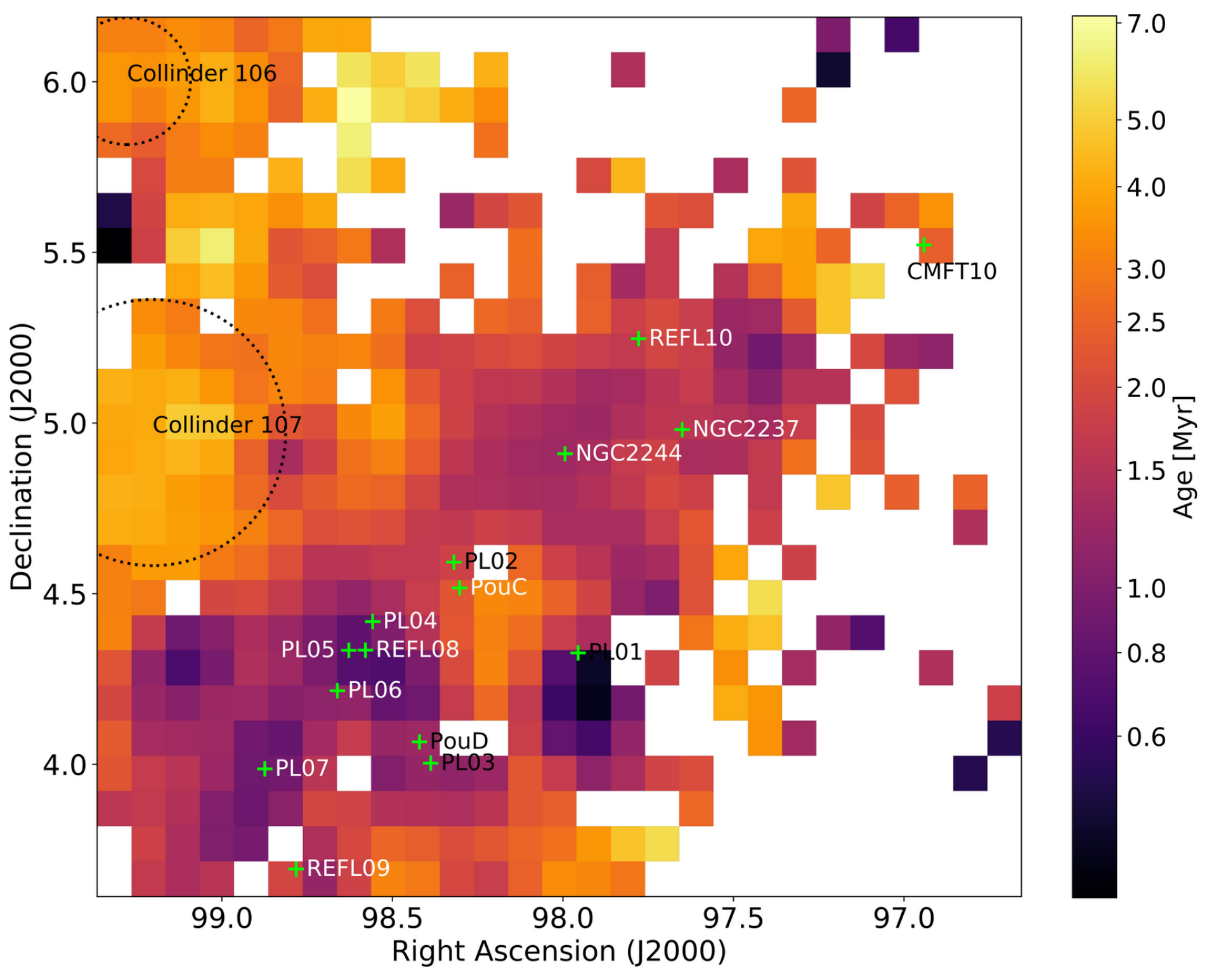

Figure 6. Map of mean ages as a function of the position on the sky, with the bin size of 6′ × 6′. The region to the South-East of NGC 2244 contains on average the youngest stars in the entire Rosette Nebula.

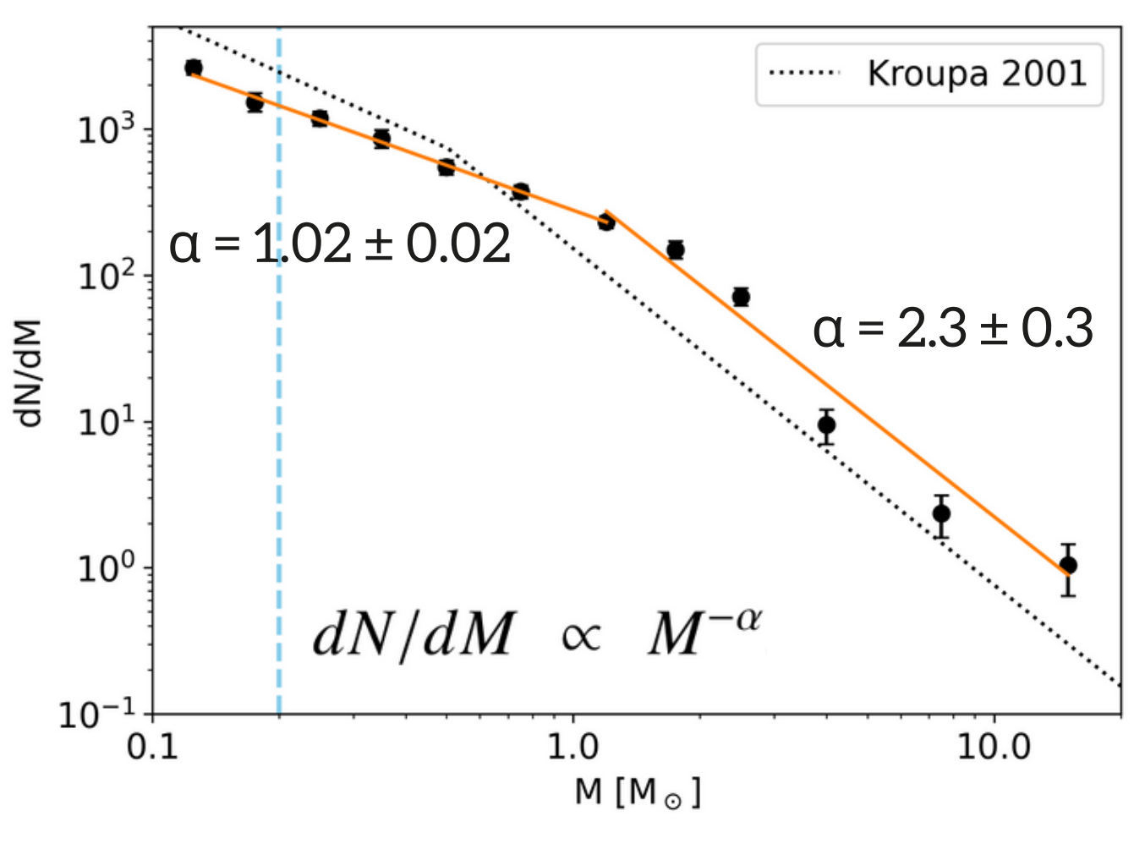

Figure 7. Initial mass function of the cluster NGC 2244 in the power-law form. The vertical blue dashed line marks the completeness limit.

Summary

distance: 1488 ± 39 pc (all)
1433 ± 35 pc (NGC 2244)
mean age: 1.6 ± 0.5 Myr (all)
1.3 ± 0.4 Myr (NGC 2244)

NGC 2244

- core radius: 2.0 ± 0.4 pc
- total mass: 1000 ± 70 M⊙
- probably unbound, possibly even formed in a super-virial state. Evidence for hierarchical formation (from the comparison with **numerical simulations**) (Parker et al. 2014, Parker & Wright 2016, Wright & Parker 2019, Bonilla Barroso et al. 2022)

References:

Bayo et al. 2008, A&A, 492, 277; Bell et al. 2013, MNRAS, 434, 806; Bonilla-Barroso et al. 2022, MNRAS, 511, 4801; Bressan et al. 2012, MNRAS, 427, 127; Kuhn et al. 2014, ApJ, 787, 107; Kuhn et al. 2021, ApJS, 254, 33; Meng et al. 2017, ApJ, 836, 34; Parker et al. 2014, MNRAS, 438, 620; Parker & Wright 2016, MNRAS, 457, 3430; Reis et al. 2019, AJ, 157, 16; Wright & Parker 2019, MNRAS, 489, 2694

This work is supported by the FCT – Fundação para a Ciência e a Tecnologia, I.P., project ID PTDC/FIS-AST/28731/2017